Hyperthermal Reactions of O and O_2 with a Hydrocarbon Surface: Direct C−C Bond Breakage by O and H-Atom Abstraction by O_2

Jianming Zhang, Hari P. Upadhyaya, Amy L. Brunsvold, and Timothy K. Minton*

Department of Chemistry and Biochemistry, Montana State University, Bozeman, Montana 59717

Received: March 12, 2006; In Final Form: April 30, 2006

A C−C bond-breaking reaction has been observed when a beam containing hyperthermal oxygen was directed at a continuously refreshed saturated hydrocarbon liquid (squalane) surface. The dynamics of this C−C bond-breaking reaction have been investigated by monitoring time-of-flight and angular distributions of the volatile product, OCH_3 or H_2CO. The primary product is believed to be the methoxy radical, OCH_3, but if this radical is highly internally excited, then it may undergo secondary dissociation to form formaldehyde, H_2CO. Either the primary or the secondary product may scatter directly into the gas phase before thermal equilibrium with the surface is reached, or they may become trapped on the surface and desorb in thermal equilibrium with the surface. Direct, single-collision scattering events that produce a C−C bond-breaking product are described with a kinematic picture that allows the determination of the effective surface mass encountered by an incident O atom, the atom−surface collision energy in the center-of-mass frame, and the fraction of the center-of-mass collision energy that goes into translation of the scattered gaseous product and the recoiling surface fragment. The dynamical behavior of the C−C bond-breaking reaction is compared with that of the H-atom abstraction reaction, which was the subject of an earlier study. Another reaction, H-atom abstraction by O_2 (which is present in the hyperthermal beam), has also been observed, and the dynamics of this reaction are compared with the inelastic scattering dynamics of O_2 and the dynamics of H-atom abstraction by O. The dynamics involving direct inelastic and reactive scattering of O_2 are also described in terms of a kinematic picture where the incident O_2 molecule is viewed as interacting with a local region of the surface.

I. Introduction

Reactions involving $O(^3P)$ in the residual atmosphere of the Earth lead to hydrocarbon material degradation on spacecraft operating in the low Earth orbital environment.[1−3] The high relative velocity between a spacecraft and the ambient O atoms gives rise to atom−surface collisions that are equivalent to $O(^3P)$ atoms with ∼450 kJ mol^{-1} of translational energy colliding with a surface.[4] The energy associated with these collisions is sufficient to overcome many reaction barriers; thus the chemistry is complex. Many recent studies are beginning to reveal the mechanisms of $O(^3P)$ reactions with model carbon[5−10] and hydrocarbon[1,8,11−20] systems at collision energies of hundreds of kJ mol^{-1}, commonly referred to as "hyperthermal" collision energies.

In our laboratory, we have studied the dynamics of hyperthermal $O(^3P)$ reactions with small alkanes in the gas phase, and the experimental results have been compared with theoretical calculations.[12,14,16] Both experiments and theory show evidence for an H-atom abstraction reaction, which has a relatively low barrier in the range 14−42 kJ mol^{-1},[21] an H-atom elimination reaction where the incident O atom binds to a carbon atom and an adjacent H atom is eliminated, and a C−C bond-breaking reaction where the incident O atom binds to a carbon atom and an adjacent C−C bond is broken.[12−17] The latter two reactions have high barriers of ∼190 kJ mol^{-1}. Theoretical calculations predict that for collision energies above 200 kJ mol^{-1} H-atom abstraction is the most probable reaction pathway. The H-atom elimination channel also occurs with a significant probability, but the C−C bond-breaking reaction is relatively improbable.

We have seen that $O(^3P)$ reactions at a saturated hydrocarbon surface show many of the same features as the gas-phase reaction dynamics. In a beam−surface scattering experiment,[1,18] in which a beam containing hyperthermal $O(^3P)$ atoms (with average translational energies of 297 and 504 kJ mol^{-1}) was directed at a continuously refreshed liquid (squalane) surface, we observed inelastically scattered O atoms and reactively scattered OH and H_2O, and we characterized the dynamics of these scattering processes. We observed that all three products could be ejected from the surface either directly, before coming into thermal equilibrium with the surface, or thermally, after having come into thermal equilibrium with the surface. The source of H_2O was determined to be secondary H-atom abstraction by a primary OH product. The dynamics of the direct (nonthermal) process to produce OH were described in the center-of-mass (CM) frame, where it was assumed that the incident O atom interacts with local region of the surface that has a finite mass. We inferred from this analysis that OH is formed through single-collision events involving a transition state with a wide range of O−H−C angles or through multiple-collision events in which the first collision creates OH and subsequent collisions of OH with the surface occur before the OH scatters inelastically from the surface. Most of the collision energy in the CM frame is partitioned into translational energy of the scattered OH and the recoiled surface fragment. The reactive scattering to produce OH thus resembles the gas-phase H-atom abstraction reaction.

* Author to whom correspondence should be addressed. E-mail: tminton@montana.edu.

10.1021/jp061521x CCC: $33.50
Published on Web 06/07/2006

The H-atom abstraction reaction between $O(^3P)$ and a hydrocarbon surface has also been studied with lower-energy O atoms. We have investigated this reaction with beam−surface scattering and mass spectrometric detection of the products (similar to our studies of hyperthermal O-atom interactions with a squalane surface),[22,23] and we found that the dynamics were qualitatively similar to those observed with hyperthermal O atoms in these studies where the O-atom translational energies were 20 and 45 kJ mol^{-1}. McKendrick and co-workers have studied this reaction with laser-based photolytic production of $O(^3P)$ above a squalane surface and laser-induced fluorescence detection of the OH product.[24−26] The average collision energy that they used was ∼15.8 kJ mol^{-1}. They proposed a direct abstraction mechanism with dynamics similar to those for analogous gas-phase reactions, and they also described a thermal OH component as a trapping−desorption process that leads to rotational equilibrium. They detected vibrationally excited OH radicals and suggested that secondary and/or tertiary H atoms may be accessible to the attacking O atoms. Hase and co-workers have performed a theoretical study of the reaction between $O(^3P)$ and an alkane thiol self-assembled monolayer (SAM) with a quantum mechanics/molecular mechanics (QM/MM) model.[27] This work focused on reactions with incident O-atom energies in the range 5−80 kJ mol^{-1}. The only primary reaction channel observed was H-atom abstraction to form OH. They observed a few trajectories in which a primary OH radical abstracted a hydrogen atom to form an H_2O molecule.

Theoretical studies have been extended to study the interactions between hyperthermal $O(^3P)$ atoms and a hydrocarbon surface. These studies have mostly focused on alkane thiol SAM surfaces,[15,17] but very recent theoretical work comes closer to the experiments by carrying out calculations for O-atom reactions with a squalane surface.[28] In the calculations with SAM and squalane surfaces, the same kinds of reactions observed in the gas phase were found to occur in the gas−surface reactions. Troya and Schatz[15,17] have performed trajectory calculations based on a QM/MM model for the reaction between hyperthermal $O(^3P)$ with an alkane thiol SAM surface. The calculation was carried out for an O-atom incident energy of 490 kJ mol^{-1}. Besides inelastic scattering of O atoms and H-atom abstraction to form OH and H_2O, they have observed additional reaction pathways, such as O-atom addition with simultaneous H-atom elimination or C−C bond breakage. The addition reactions, especially H-atom elimination, compete with H-atom abstraction to form OH, even though the addition processes have much higher barriers.

Our earlier beam−surface studies focused on O-atom energy transfer at a hydrocarbon surface and the reactions that involved H-atom abstraction.[18] We have now revisited this system in light of newer experimental and theoretical evidence for the previously unobserved addition reaction pathways, with the specific goal of identifying and describing the dynamics of the H-atom elimination and C−C bond-breaking reactions. A hyperthermal beam containing O and O_2 was directed at a continuously refreshed liquid squalane surface, and the product translational energy and flux distributions were measured as functions of incident angle and detection, or final, angle. We found that our experimental technique was not sensitive to the H-atom elimination channel; however, we did observe products indicative of the C−C bond-breaking reaction, and we have mapped out the dynamics of this reactive process in this paper. In the process of conducting our experiments, we identified another reaction, H-atom abstraction by O_2, which was present in our hyperthermal beam, and we have also described the dynamics of that process.

II. Experimental Details

The experiments were performed with the use of a crossed molecular beams apparatus[29−31] that was coupled to a laser detonation hyperthermal beam source[32] and configured for beam−surface scattering experiments. The experimental setup was very similar to that reported in detail in a previous paper.[18] Briefly, a pulsed beam containing hyperthermal O and O_2 was directed at a hydrocarbon surface, and a rotatable mass spectrometer detector was used to monitor the scattered products. The rotation axis of the detector passed along the surface and was coincident with the rotation axis of the surface. The surface normal and detector therefore rotated in the same plane. Reactively and inelastically scattered species that emerged from the surface were detected as a function of incident angle, θ_i, and final angle, θ_f, with respect to the surface normal. To characterize the hyperthermal beam, the surface was lowered out of the beam path, and the beam was directed into the detector. Measurements of the beam were used to determine the velocity distributions of the components of the beam and their relative fluxes.

The pulsed hyperthermal beam, which operated at a repetition rate of 2 Hz, contained atomic and molecular oxygen. The fraction of atomic oxygen was about 85%, and the atomic oxygen was in its ground electronic state, $O(^3P)$.[33] A synchronized chopper wheel was used to select a narrow portion of the hyperthermal beam pulse. The average (laboratory) translational energy of the O atoms in the beam was 510 kJ mol^{-1}, with an energy width (full width at half-maximum) of 70 kJ mol^{-1}. The molecular oxygen in the beam was also in its ground state, $O_2(^3\Sigma_g^-)$,[31] and had an average translational energy of 1020 kJ mol^{-1} and width of 140 kJ mol^{-1}.

The beam was directed at a continuously refreshed liquid squalane surface, which ensured that only the initial reactions between the incident beam and the surface were being probed. Squalane ($C_{30}H_{62}$, 2,6,10,15,19,23-hexamethyltetracosane) is a partially branched saturated hydrocarbon and is a liquid at room temperature, with a vapor pressure of $\sim 2 \times 10^{-8}$ Torr. The temperature of the squalane surface was maintained at 10 °C during the experiment. This temperature, which was lower than ambient, was found to reduce the background signal in the detector from the evaporation of squalane.

The number density distributions of scattered products from the surface were collected as a function of arrival time in the electron impact ionizer of the detector, which was 33.7 cm from the surface. These distributions, referred to as time-of-flight (TOF) distributions, were collected at a variety of final angles for two angles of incidence, $\theta_i = 30°$ and 60°. The main focus of the work presented here was on the C−C bond-breaking reaction that produced a signal identified as either OCH_3 or H_2CO. The initial product is presumed to be in the form of the methoxy (OCH_3) radical because of the substantial evidence for this product in theoretical studies of hyperthermal reactions of $O(^3P)$ with alkanes.[13−17] However, a fraction of the methoxy products might have dissociated to H_2CO before reaching the detector. Signals indicative of a methoxy radical product were detected at $m/z = 28$ (CO^+), 29 (CHO^+), and 30 (CH_2O^+). The background signals at $m/z = 28$ and 29 were significantly higher than the background signal at $m/z = 30$. The high background signals at $m/z = 28$ and 29 are the result of dissociative ionization of evaporated squalane in the detector, which yielded

significant fragments at $C_2H_4^+$ and $C_2H_5^+$. In addition, some collision-induced processes at the squalane surface, which most likely resulted from energetic O_2 collisions, also gave rise to signals at relatively large flight times, and these signals interfered with the methoxy signal. The collision-induced processes will be discussed further in the next section. Time-of-flight distributions were also collected at $m/z = 15$ and 31, which could be representative of the methoxy product with ionizer fragments CH_3^+ and CH_3O^+. However, signals at $m/z = 15$ and 31 were determined to originate from inelastically scattered O and O_2, which could be detected at $m/z = 15$ and 31, respectively, because of the finite resolution of the mass spectrometer. Therefore, the key mass-to-charge ratio for our studies, which focused on the presumed methoxy reaction product, was 30. For each incident angle, TOF distributions at $m/z = 30$ were accumulated for a total of 4000 beam pulses at each final angle. During the collection of the TOF distributions, the final angle was incremented until the entire (incident-angle-dependent) angular range was covered. Then the increment direction was reversed, and the cycle was repeated until a total of four TOF distributions (each accumulated for 1000 beam pulses) had been recorded for every final angle. The four distributions corresponding to each final angle were then summed to yield a TOF distribution whose relative magnitude and shape were virtually unaffected by long-term drifts in the experimental parameters.

Time-of-flight distributions corresponding to other possible beam−surface reaction products were also collected for various incident and final angles. The presence of other potential C−C bond-breaking products, such as OCH_2CH_3, $OCH(CH_3)_2$, and $OCH_2CH(CH_3)_2$, was investigated by collecting TOF distributions at $m/z = 40$, 41, 42, 43, 44, 45, and 46, $m/z = 52$, 53, 54, 55, 56, 57, 58, and 59, and $m/z = 64$, 65, 66, 67, 68, 69, 70, 71, 72, and 73, respectively. Efforts were also made to detect signals at $m/z = 1$, which could arise from an H-atom elimination reaction analogous to H-atom elimination reactions that have been observed in gas-phase studies of hyperthermal $O(^3P)$ reactions with alkanes. In the process of identifying all observable reactions between the hyperthermal beam and the squalane surface, we discovered a reaction involving H-atom abstraction by O_2. We investigated the dynamics of this reaction by collecting TOF distributions at $m/z = 32$ (O_2^+) and 33 (HO_2^+) in a similar manner as the TOF distributions for $m/z = 30$ were collected. While we observed signals at mass-to-charge ratios corresponding to inelastically scattered O ($m/z = 16$) and reactively scattered OH ($m/z = 17$) and H_2O ($m/z = 18$), we did not study these products closely, as their dynamical behavior was the focus of an earlier study.[18]

III. Results and Analysis

A. H-Atom Elimination Reaction. Great efforts were made to detect an H-atom signal at $m/z = 1$. Figure 1 shows the TOF distributions for $m/z = 1$ and 17 collected when the incident angle, θ_i, was 60° and the final angle, θ_f, was either 60° or 20°. Comparison of the TOF distributions for $m/z = 1$ and 17 shows that the majority of the fast component (with a peak near 90 μs) of the signal at $m/z = 1$ is from dissociative ionization of OH. Dissociative ionization of other H-containing products, mainly H_2O, contributes to the slow component (~450 μs) of the signal at $m/z = 1$. Assuming a substitution reaction, analogous to that observed in gas-phase studies,[12−17] which leads to volatile H-atom products, then a signal from the H atoms would be expected at flight times in the vicinity of 25 μs. This flight time would correspond to about 100 kJ mol^{-1} of translational energy in the H atoms. We were, however, unable

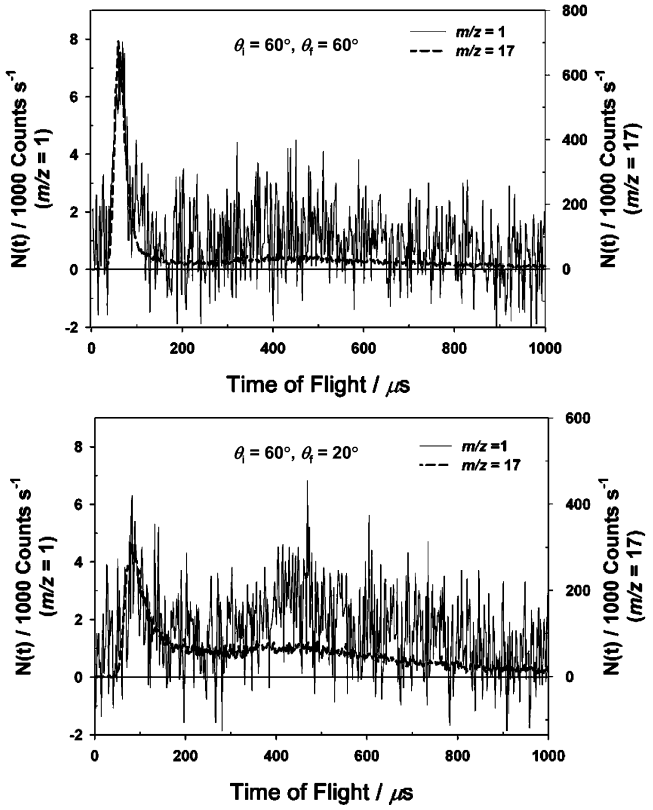

Figure 1. Time-of-flight distributions of $m/z = 1$ and 17 collected with $\theta_i = 60°$ and $\theta_f = 60°$ and 20°.

to identify any signal at $m/z = 1$ that could be the result of an H-atom elimination reaction. Unfortunately, the high background at $m/z = 1$ and the low detection sensitivity of H, resulting from its relatively high velocity and low ionization cross section, made it impossible to determine whether such a reaction was occurring.

B. C−C Bond-Breaking Reactions and the Production of OCH_3. Other than the simplest C−C bond-breaking product, OCH_3, possible C−C bond-breaking products include OCH_2CH_3, $OCH(CH_3)_2$, and $OCH_2CH(CH_3)_2$, corresponding to $m/z = 45$, 59, and 73, respectively. Figure 2 shows TOF distributions that were detected at $m/z = 29$, 43, 57, 71, and 85, when $\theta_i = 60°$ and $\theta_f = 60°$. Time-of-flight distributions at other mass-to-charge ratios, such as $m/z = 40$, 41, 42, 44, 45, 46; 52, 53, 54, 55, 56, 58, 59; 64, 65, 66, 67, 68, 69, 70, 72, and 73, are similar to those shown in Figure 2 for all the mass-to-charge ratios higher than 29. The TOF distribution at $m/z = 29$ is unique in its hyperthermal component (~150 μs), which must have a different origin than any of the signals observed at higher mass-to-charge ratios. The TOF distributions corresponding to products with $m/z > 40$ at other masses do not have hyperthermal components. The slow, broad signals with flight times around 1300 μs can only be explained by ionizer fragmentation of evaporated squalane molecules. In fact, $m/z = 43$, 57, 71, and 85 correspond to the four highest peaks of the mass spectrum of the squalane molecule at an electron energy of 70 eV.[34] Low-molecular-weight reaction products ($m/z < 100$) that leave the surface with thermal velocities (corresponding to 283 K) when the beam pulse strikes the surface would be expected to arrive at the detector at much shorter times, between 500 and 1000 μs. The steady-state evaporation of squalane molecules produces a continuous high background at all the mass-to-charge ratios presented in Figure 2. However, the fact that squalane signals are observed above the background level for a short time

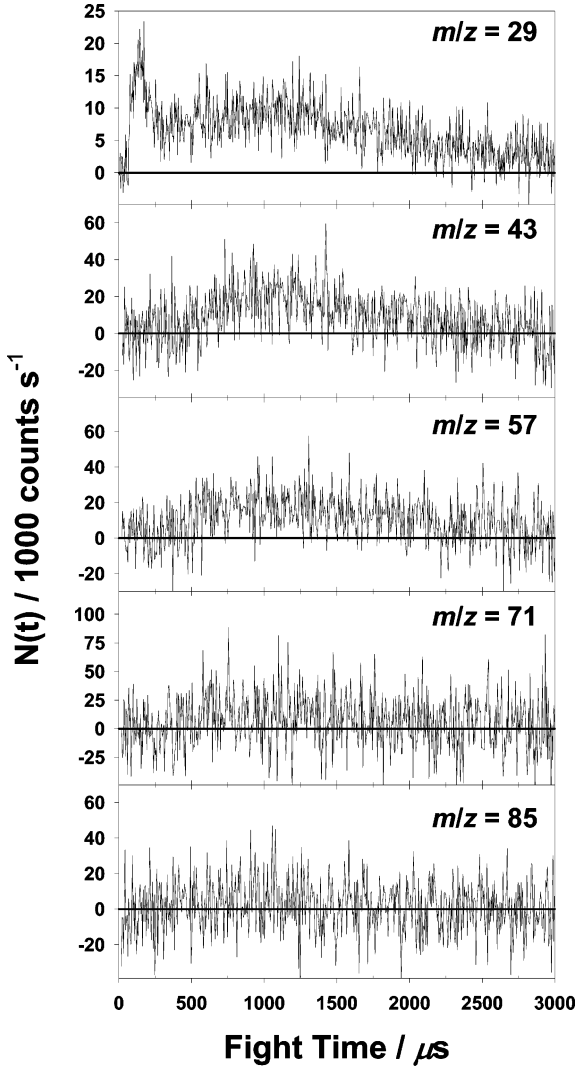

Figure 2. Time-of-flight distributions of $m/z = 29$, 43, 57, 71, and 85 collected with $\theta_i = 60°$ and $\theta_f = 60°$.

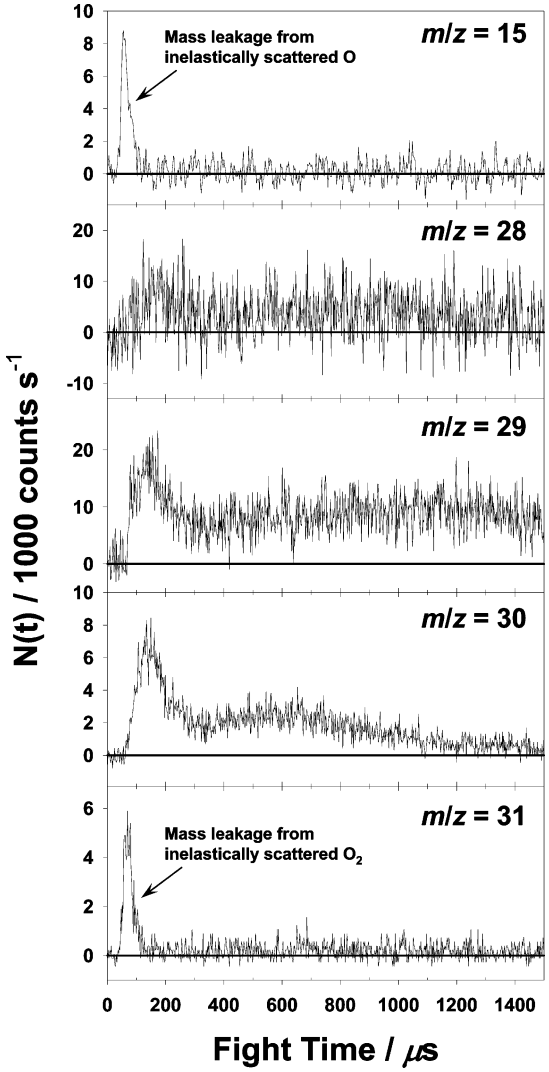

Figure 3. Time-of-flight distributions of $m/z = 15$, 28, 29, 30, and 31 collected with $\theta_i = 60°$ and $\theta_f = 60°$.

just after a beam pulse strikes the surface suggests that collision-induced evaporation of squalane is producing these transient signals. A similar phenomenon has also been observed in our study of collision-induced dissociation of perfluoropolyether (PFPE) with hyperthermal Ar beams.[35] Because all TOF distributions collected at $m/z > 40$ only show slow, broad signals attributable to collision-induced evaporation of squalane, we conclude that the peak at short times in the TOF for $m/z = 29$ arises from a product that contains one carbon atom and one oxygen atom. This product was initially assigned to the methoxy radical by inference from the related computational studies on hyperthermal $O(^3P)$ reactions with gaseous alkane molecules and with hydrocarbon self-assembled monolayer surfaces.[12−17] The signal detected at long times (~1300 μs) in the $m/z = 29$ TOF distribution is still explained by collision-induced evaporation of squalane.

Further work was done to ensure that the unique signal observed at $m/z = 29$ was not the result of dissociative ionization of a higher-mass, oxygen-containing product. We note that the background level at $m/z = 29$ is about 70 000 counts/s, approximately 3 times higher than the CH_3O signal level at this mass. However, the background levels at $m/z = 43$, 57, and 71 are much higher, varying between 1 and 2 million counts/s. Therefore, even if the signal levels of OCH_2CH_3, $OCH(CH_3)_2$, or $OCH_2CH(CH_3)_2$ were similar to that of OCH_3, the high background levels (40−85 times the signal level) might result in the reactive signal going unnoticed. To determine whether oxygen-containing products with masses higher than 40 were formed, we counted for exceedingly long times (5 times longer than that for $m/z = 29$), for example, 10 000 beam pulses for $m/z = 43$, and concluded that these products would have to have signal levels less than 10% that of the hyperthermal signal at $m/z = 29$ to escape notice. The obvious signal detected at $m/z = 29$ is almost certainly, then, dominated by a product consisting of one carbon atom and one oxygen atom.

Such a product might be methoxy (OCH_3) or hydroxymethyl (CH_2OH). Formaldehyde (H_2CO) is another possible product, although if formed, it would likely be the result of secondary dissociation of nascent methoxy or hydroxymethyl that is internally excited. To distinguish between these products, TOF distributions for $m/z = 15$, 28, 29, 30, and 31 were collected with $\theta_i = 60°$ and $\theta_f = 60°$ and compared (Figure 3). The TOF distributions for $m/z = 15$ and 31 show significant sharp signals that are attributed to mass leakage from inelastically scattered O and O_2, respectively. The TOF distributions for $m/z = 15$ and 31 show no sign of signal at flight times (~150 μs) corresponding to the presumed OCH_3 product. However, it cannot be ruled out that even an intact methoxy product might go undetected at $m/z = 15$, as the background level is about 80 000 counts/s and the product is expected to have a relatively

small cross section for being detected at this mass-to-charge ratio. The lack of reactive signal at $m/z = 31$ suggests that CH_2OH is not an important product. CH_2OH^+ is a relatively stable ion, so we would expect to observe signal at the parent mass, $m/z = 31$, if CH_2OH were formed. However, OCH_3 is not expected to produce a parent ion at $m/z = 31$, but this species will be detected at $m/z = 15$, 28, 29, and 30.[36,37] The fast components ($\sim$150 μs) for the TOF distributions of $m/z = 28$, 29, and 30 have very similar shapes and flight times, indicating that they originate from the same product. The fragmentation pattern is, however, not indicative of the OCH_3 radical.[37] The fragmentation pattern is closer to that expected for H_2CO. Additional weight is given to the idea that H_2CO is the observed product by the $m/z = 15$ TOF distribution, which shows no signal from CH_3^+. Nevertheless, theoretical calculations suggest that direct formation of H_2CO is either highly improbable or impossible for reactions of hyperthermal $O(^3P)$ with methane, ethane, or propane.[13−16] We thus conclude that secondary dissociation of nascent OCH_3 to H_2CO is a likely explanation for the observed signals. Another possibility is that some fraction of highly excited OCH_3 products survives to the detector, where the high internal excitation results in a fragmentation pattern that is different from what was previously observed.[37] On the basis of the signals observed at $m/z = 15$, 28, 29, 30, and 31 as well as the relative intensities of these signals, we are left with the possibilities that (a) all nascent OCH_3 products are formed with enough internal energy to dissociate to H_2CO or (b) some fraction of nascent OCH_3 products dissociate to H_2CO and some fraction of OCH_3 products survive to the detector.

In either case, the observed dynamical behavior of the hyperthermal signal can be assumed to represent the nascent OCH_3 product. A similar conclusion was reached in studies of the hyperthermal reactions of $O(^3P)$ with CH_4[16] and CD_4.[38] For the case of $O(^3P) + CH_4$, the collision energy was 280 kJ mol^{-1}, and weak signals at $m/z = 15$ (CH_3^+) and 31 (CH_3O^+) were detected, indicating the presence of nascent OCH_3 and, possibly, a small fraction of secondary isomerization to CH_2OH. However, the reaction of $O(^3P) + CD_4$ had a higher collision energy, 305 kJ mol^{-1}, and no signals were detected at $m/z = 18$ (CD_3^+) and 34 (CD_2OD^+). This trend is consistent with the observations in the reaction with squalane, which has much higher collision energy (>400 kJ mol^{-1}). Thus, much higher internal energy is probably available for nascent OCH_3, leading to more complete secondary dissociation and less or no isomerization. The secondary H_2CO should still reflect the dynamics of the nascent OCH_3, because H_2CO recoils very slowly from a light H-atom counter fragment; therefore, both the nascent OCH_3 and the secondary H_2CO will scatter with approximately the same directions and velocities in the laboratory reference frame.

The TOF distributions for $m/z = 28$ and 29 (Figure 3) show very slow components at flight times around 1300 μs, which is much slower and broader than the expected flight times ($\sim$600 μs) for OCH_3 that scatters with velocities corresponding to the surface temperature of 283 K. As discussed above, these slow signals originate from squalane molecules, and they interfere with the signals from OCH_3. The steady-state background levels at $m/z = 28$, 29, and 30 are about 125 000, 70 000, and 1000 counts s^{-1}, respectively. Even though the signal level at $m/z = 29$ is the highest for the product assumed to represent nascent OCH_3, the background, both steady-state and transient, at $m/z = 30$ is so low that this mass-to-charge ratio provided the most effective window into the dynamics of the C−C bond-breaking reaction to produce nascent OCH_3.

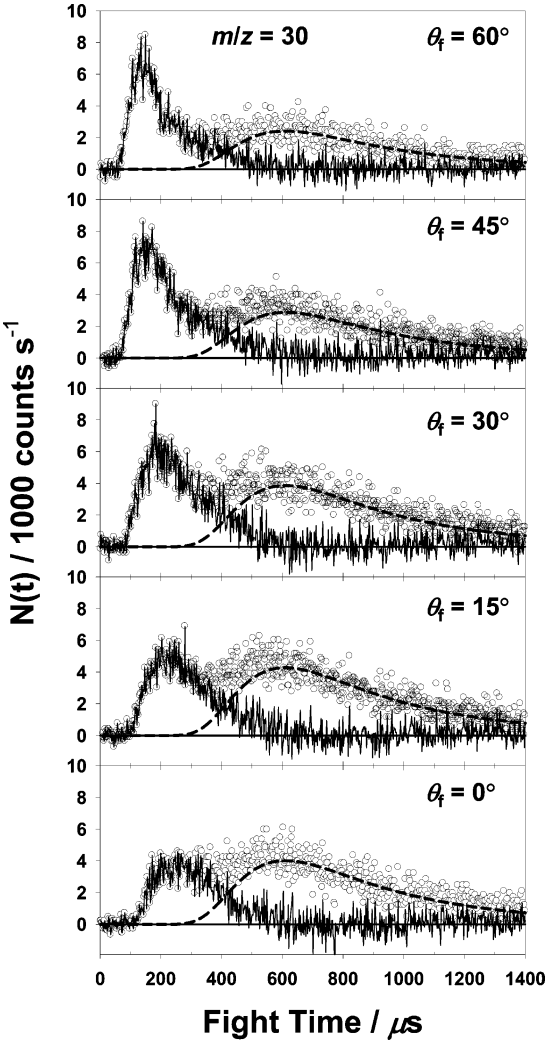

Figure 4. Representative time-of-flight distributions of reactively scattered OCH_3 collected with $\theta_i = 60°$ and $\theta_f = 60°$, 45°, 30°, 15°, and 0°. The dashed curves represent the thermal (Maxwell−Boltzmann) components, and the solid curves represent the hyperthermal components, which come from the differences between the overall distributions (circles) and the thermal components.

Figure 4 shows representative TOF distributions for the C−C bond-breaking product detected at $m/z = 30$. These distributions were collected with an angle of incidence of 60°; distributions for five final angles are shown. All the TOF distributions appear bimodal, indicating two distinct processes. The slower (longer flight times) component corresponds to products that scatter from the surface with a Maxwell−Boltzmann distribution of velocities given by the surface temperature. The faster (shorter flight times) component corresponds to products that scatter from the surface at velocities significantly greater than those given by the surface temperature. The slower products are therefore often referred to as thermal products, while the faster products are referred to as hyperthermal products. For a given incident angle, the intensity of the hyperthermal component generally increases with final angle, reaches a maximum, and then decreases. The intensity of the thermal component always decreases with final angle. The bimodal TOF distributions suggest that some of the initially formed OCH_3 (or H_2CO) products are in thermal equilibrium with the surface before desorbing (trapping desorption), while the rest emerge from the surface on a time scale too short for thermal equilibrium to be achieved (direct reaction). As the barrier for the formation of OCH_3 through C−C bond breakage is $\sim$190 kJ mol^{-1}, the

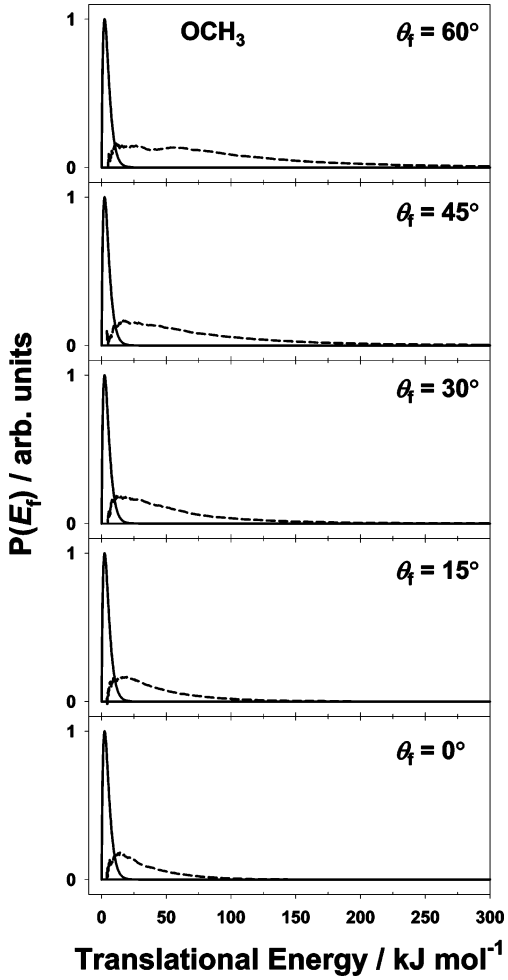

Figure 5. Translational energy distributions of reactively scattered OCH_3 derived from the time-of-flight distributions shown in Figure 4. Each panel shows thermal (solid curves) and hyperthermal (dashed curves) components.

thermal OCH_3 products cannot originate from reactions with trapped (thermal) O atoms on the surface. Therefore, the thermal OCH_3 (or H_2CO) products must come from directly formed products, which then become trapped. Each TOF distribution was used to derive two product translational energy distributions: one for trapping desorption and the other for direct reaction. This analysis was conducted in a manner, described earlier,[18,39] which takes into account the fact that the detector is a number density detector and assumes a monoenergetic incident beam and an infinitely small ionizer length. The slower component was first fit with a Maxwell−Boltzmann distribution at the surface temperature. The difference between the overall TOF distribution and the assumed Maxwell−Boltzmann component was taken to be the TOF distribution of the hyperthermal component. This TOF distribution was then inverted to yield a translational energy distribution for the hyperthermal products that scattered at a particular final angle. Figure 5 shows the translational energy distributions (probability density distributions as a function translational energy, $P(E_T)$) that were derived from the TOF distributions in Figure 4. The peak of each Maxwell−Boltzmann energy distribution has been normalized to one, and the areas of each pair of distributions are proportional to the respective fluxes of OCH_3 that scattered through the two processes at a given final angle. The average energies of OCH_3, which scattered directly (hyperthermal component) at each final angle, were calculated for the two incident angles and are plotted as a function of final angle in Figure 6. As can be seen, the

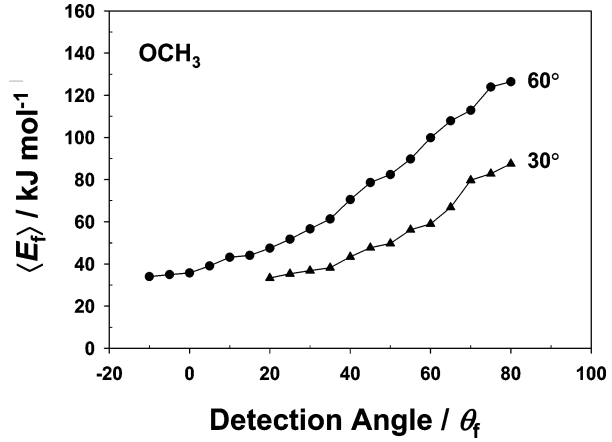

Figure 6. Average final translational energies of hyperthermal OCH_3 as a function of detection angle for $\theta_i = 60°$ and 30°.

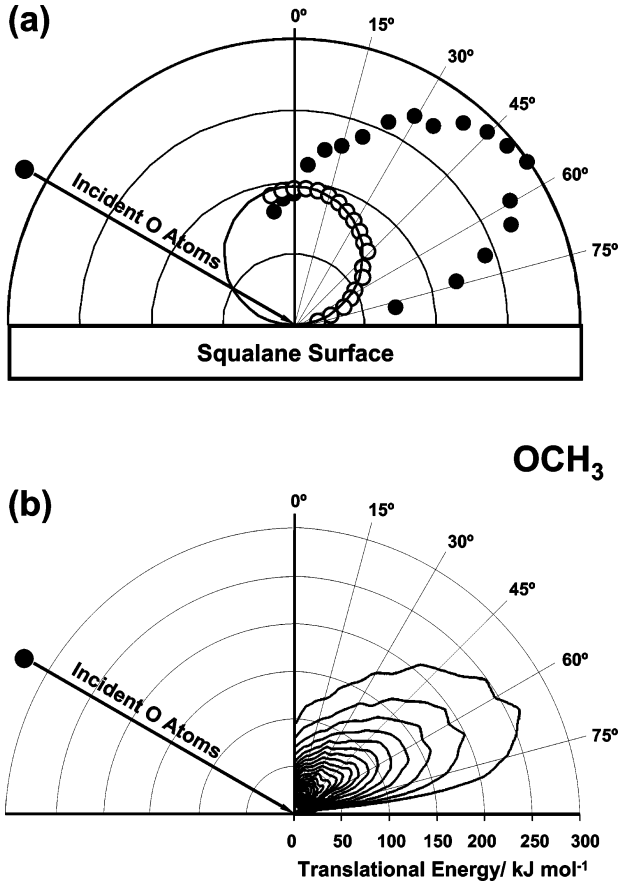

Figure 7. (a) Flux distributions of thermal (open circles) and hyperthermal (solid circles) components as a function of final angle for reactively scattered OCH_3, with $\theta_i = 60°$. The solid line is the cos θ_f fit to the thermal component. (b) Contour map, showing translational energy and flux of OCH_3 as a function of final angle, with $\theta_i = 60°$.

average final translational energy of the hyperthermal products increases with final angle, and an increase in incident angle appears to lead to a general increase in final energies.

Figure 7a shows angular distributions of scattered OCH_3 flux for an incident angle of 60°. The combination of the angular distributions and the translational energy distributions provides a contour map of final energy and flux as a function of detection angle, as shown in Figure 7b. The hyperthermal product angular distribution is far from cosine, with a maximum at an angle slightly less than the specular angle. However, the thermal products do follow a cos θ_f distribution.

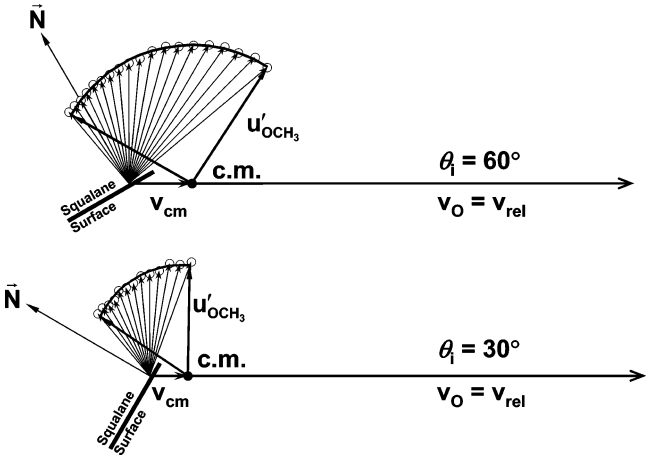

Figure 8. Simple Newton diagrams for reactive scattering of OCH_3 (hyperthermal components) following the impact of O atoms with a squalane surface at $\theta_i = 60°$ and 30°. The arrows represent average velocities.

TABLE 1: Center-of-Mass Quantities Derived from a Kinematic Analysis of Reactive Scattering of OCH_3 (Hyperthermal Component) Following Impact of O Atoms with $\theta_i = 60°$ and 30° on a Squalane Surface

incident angle	effective surface mass	collision energy	total final translational energy	total final internal energy
θ_i	m_s (amu)	$\langle E_{coll} \rangle$ (kJ mol^{-1})	$\langle E_T \rangle$ (kJ mol^{-1})	$\langle E_{int} \rangle$ (kJ mol^{-1})
60°	124	451	77	374
30°	190	472	40	432

The OCH_3 products that are formed through a direct reaction (hyperthermal products) exhibit dynamical behavior that may be described in terms of a gas-phase-like process where an incident O atom is viewed as interacting with a localized region of the surface. We have previously described similar behavior for inelastically scattered O and reactively scattered OH with a kinematic analysis that employs a Newton diagram to relate the observed scattering in the laboratory reference frame to scattering in the CM frame.[1,18] Figure 8 shows Newton diagrams for reactively scattered OCH_3 following the impact of O atoms on the surface at incident angles of 60° and 30°. Average final velocities of hyperthermal OCH_3 at each final angle were used to construct these Newton diagrams. The values of the effective surface mass, the CM collision energy, and the total CM energy that goes into translation and internal motion of the scattered volatile product and the recoiling surface fragment have been derived and are presented in Table 1.

C. H-Atom Abstraction by O_2. The O_2 molecules in the hyperthermal beam were found to react by an H-atom abstraction reaction to produce HO_2. This product was detected at $m/z = 33$ (HO_2^+). To rule out the production of H_2O_2, TOF distributions were also collected at $m/z = 32$ and 34. Figure 9 shows representative TOF distributions for $m/z = 32$, 33, and 34 with $\theta_i = 60°$ and $\theta_f = 60°$. The TOF distribution for $m/z = 34$ has the same shape and temporal profile as that for $m/z = 32$, suggesting that the signal detected at $m/z = 34$ is actually from $^{16}O^{18}O$ and not H_2O_2. In addition, the flux ratio of the signals detected at $m/z = 32$ and 34 matches the natural abundance ratio expected for $^{16}O^{16}O/^{16}O^{18}O$. Furthermore, the slow, broad signal in the TOF distributions for $m/z = 32$ and 34 may be explained by residual O_2 molecules from the beam pulse that slowly effuse out of the source chamber and into the main scattering chamber, where they then make their way into the detector. These thermal O_2 molecules do not possess sufficient energy to abstract H atoms. Therefore, the TOF distribution for $m/z = 33$, which apparently originates only from HO_2 reaction products, does not have a slow tail from effused O_2.

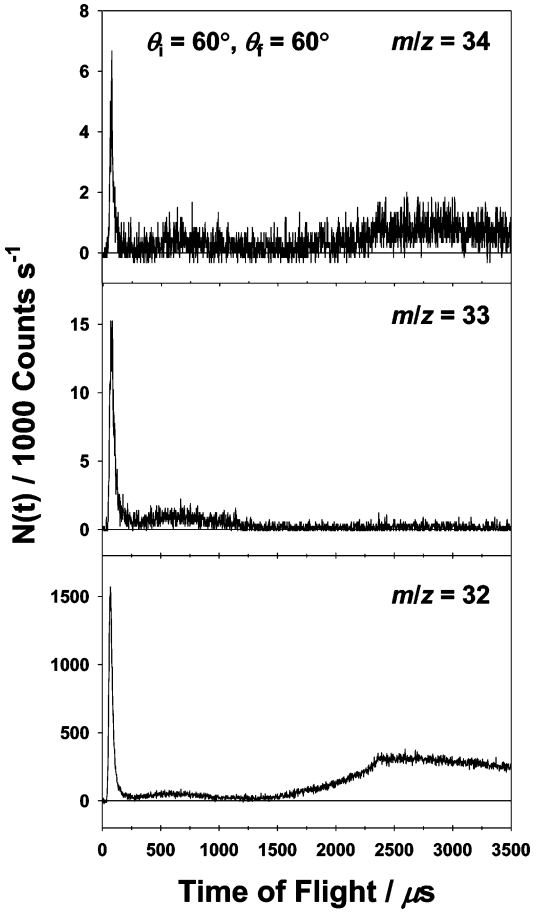

Figure 9. Time-of-flight distributions of $m/z = 34$, 33, and 32 collected with $\theta_i = 60°$ and $\theta_f = 60°$.

Figure 10 shows representative TOF distributions for $m/z = 32$ and 33 collected with $\theta_i = 60°$ and $\theta_f = 60°$, 30°, and 0°. The shapes of the TOF distributions for $m/z = 32$ and 33 look similar. As seen in the TOF distributions for OCH_3, the TOF distributions have two components, hyperthermal and thermal, with the thermal components being described well by Maxwell−Boltzmann distributions at the surface temperature. Figure 11 shows the average translational energy of the hyperthermal components of O_2 and HO_2 as a function of final angle for incident angles of 60° and 30°. The average final translational energies increase with final angle and also with incident angle (for a given final angle). The average translational energies of HO_2 are approximately 75% of those of O_2. Figures 12 and 13 show the angular distributions and contour maps of scattered O_2 and HO_2 flux, respectively, for an incident angle of 60°. The hyperthermal product angular distributions are far from cosine, with maxima in the vicinity of the specular angle, while the thermal products follow cos θ_f distributions. For HO_2, the fraction of thermal scattering is higher than that for O_2. In addition, the angular distribution for HO_2 is broader than the O_2 angular distribution. Figure 14 shows the Newton diagrams for scattered O_2 and HO_2 for $\theta_i = 60°$. Newton diagrams for $\theta_i = 30°$ have been constructed but are not shown. The values of the effective surface mass, the CM collision energy, and the total CM energy that goes into translational and internal motion of the scattered volatile product and the recoiling surface fragment were derived and are listed in Table 2.

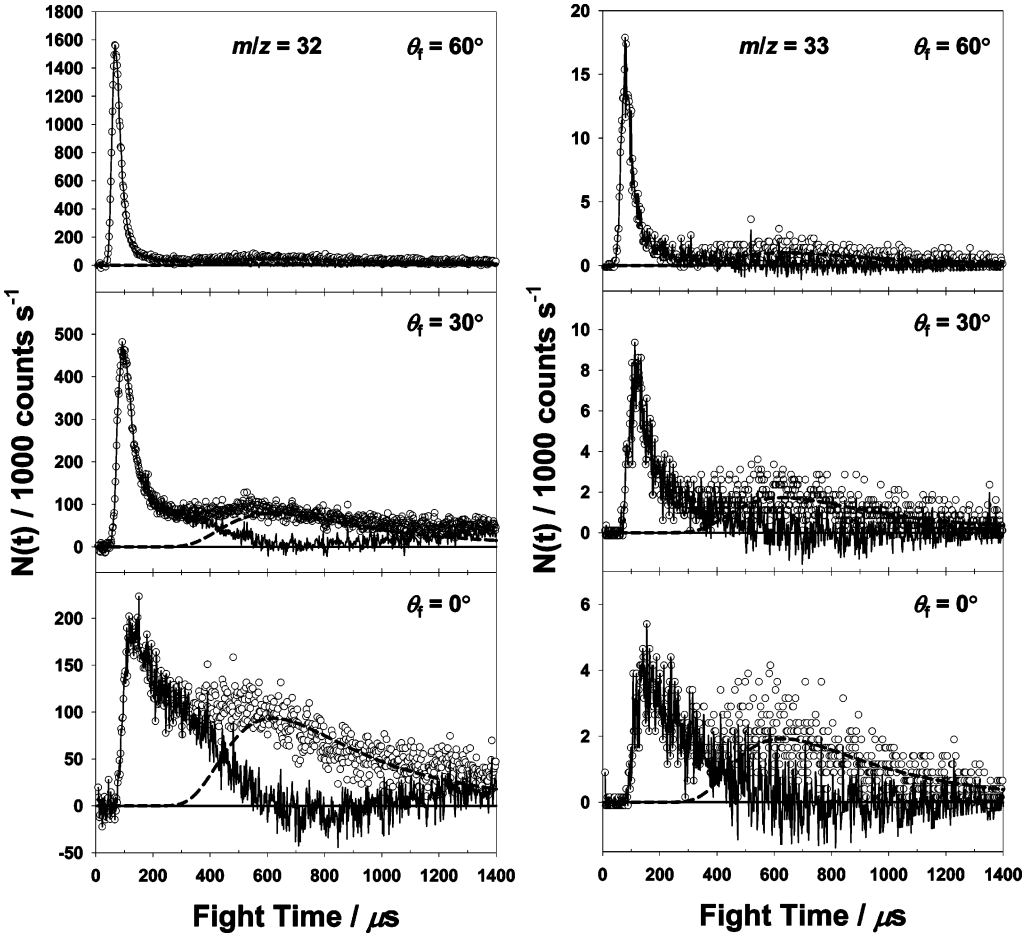

Figure 10. Representative time-of-flight distributions of inelastically scattered O_2 ($m/z = 32$) and reactively scattered HO_2 ($m/z = 33$) collected with $\theta_i = 60°$ and $\theta_f = 60°$, 30°, and 0°. The dashed curves represent the thermal (Maxwell−Boltzmann) components, and the solid curves represent the hyperthermal components, which come from the differences between the overall distributions (circles) and the thermal components.

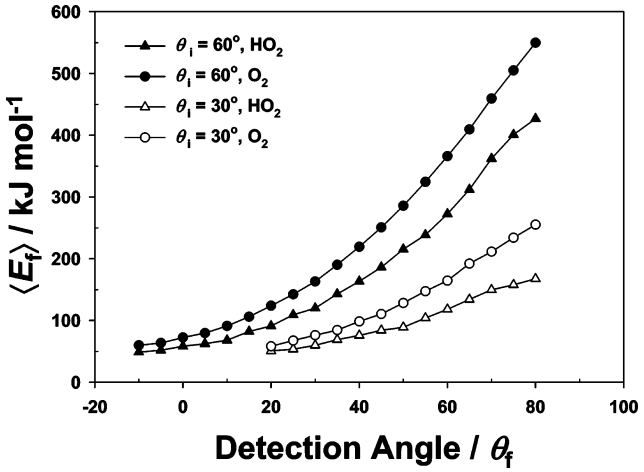

Figure 11. Average final translational energies of hyperthermal O_2 and HO_2 as a function of detection angle for $\theta_i = 60°$ and 30°.

IV. Discussion

A. O(^{3}P) Reaction with Squalane To Produce OCH_3. Although we have observed evidence for a C−C bond-breaking reaction to produce OCH_3, this is not the dominant reaction when hyperthermal O(^{3}P) atoms strike a squalane surface. At relatively low CM collision energies (<190 kJ mol^{-1}), the only open reaction channel when O(^{3}P) collides with an alkane is H-atom abstraction. At higher collision energies, additional reaction channels may be open, such as H-atom elimination and C−C bond breakage.[12−17] Theoretical calculations of the reactions between hyperthermal O(^{3}P) atoms and a hydrocarbon self-assembled monolayer (SAM) surface show that between 42% and 78% of the reactive collisions result in H-atom abstraction, while 2−15% of the reactive collisions involve C−C bond breakage.[15,17] The H-atom elimination reaction is between 16% and 53% of the total reactive events. Recent theoretical calculations of hyperthermal O(^{3}P) reactions with a squalane surface produced similar results: 49% H-atom abstraction, 43% H-atom elimination, and 2.6% C−C bond breakage, averaged over three angles of incidence, $\theta_i = 30°$, 45°, and 60°.[28] The H_2O formation channel, which has been observed in the calculations (and also in our earlier experiments with squalane), originates from an initial H-atom abstraction reaction. The C−C bond-breaking and H-atom elimination reaction channels are thus important pathways for reactions of hyperthermal O(^{3}P) atoms with hydrocarbon surfaces. In our studies of reactions of hyperthermal O(^{3}P) with a squalane surface, OH, H_2O, and OCH_3 have been observed as the reaction products. By taking into account integrated scattered flux in the scattering plane as well as relative ionization cross sections, we estimate that the relative reaction probabilities to produce OH, H_2O, and OCH_3 are 77:20:3, respectively, for an angle of incidence of 60°. As H-atom abstraction is the origin of the H_2O product, our estimate suggests that the ratio of initial H-atom abstraction events to C−C bond-breaking events is 97:3. This ratio falls within the prediction from the theoretical calculations of O(^{3}P) reactions with a hydrocarbon SAM surface. The calculations for hyperthermal O(^{3}P) reactions with SAM and squalane surfaces suggest that H-atom elimination is an important process. However, as

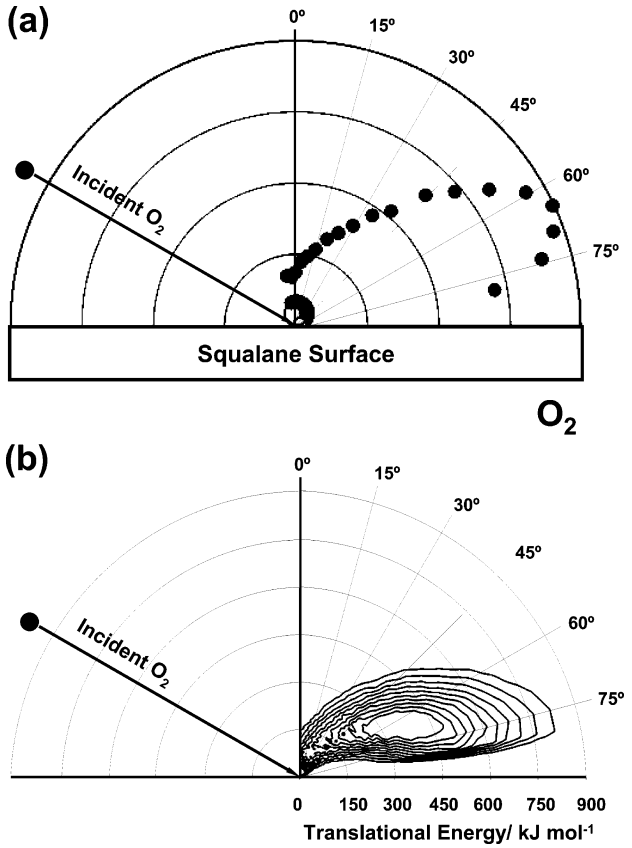

Figure 12. (a) Flux distributions of thermal (open circles) and hyperthermal (solid circles) components as a function of final angle for inelastically scattered O_2, with $\theta_i = 60°$. The solid line is the cos θ_f fit to the thermal component. (b) Contour map, showing translational energy and flux of O_2 as a function of final angle, with $\theta_i = 60°$.

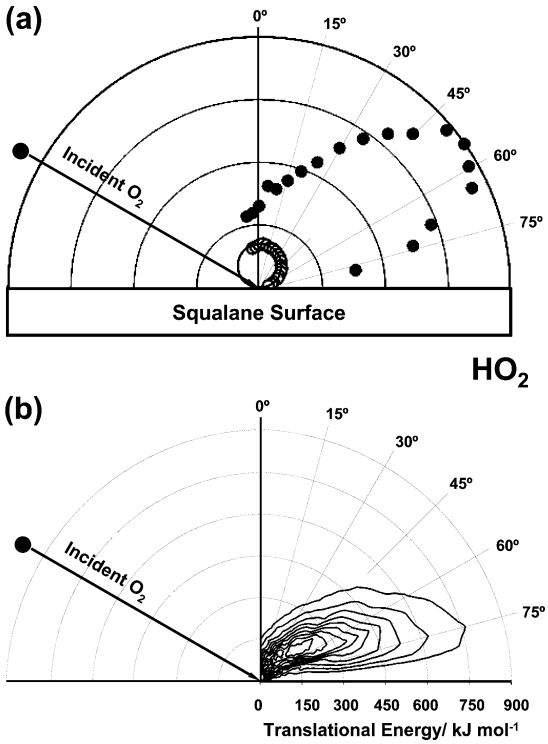

Figure 13. (a) Flux distributions of thermal (open circles) and hyperthermal (solid circles) components as a function of final angle for reactively scattered HO_2, with $\theta_i = 60°$. The solid line is the cos θ_f fit to the thermal component. (b) Contour map, showing translational energy and flux of HO_2 as a function of final angle, with $\theta_i = 60°$.

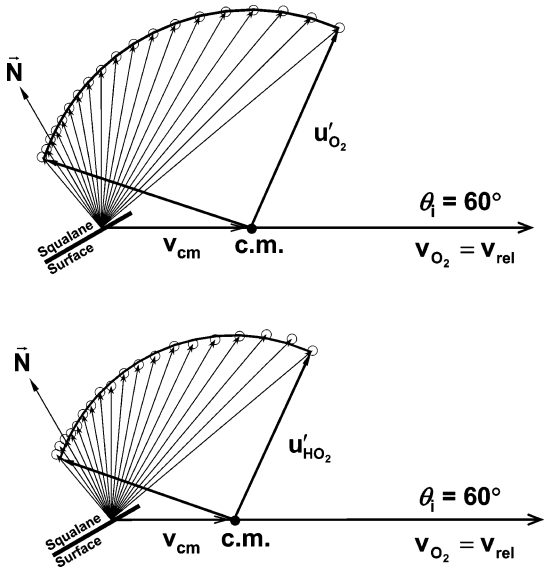

Figure 14. Simple Newton diagrams for inelastic scattering of O_2 and reactive scattering of HO_2 (hyperthermal components) following impact of O_2 with a squalane surface at $\theta_i = 60°$. The arrows represent average velocities.

discussed in section III.A, we were unable to observe evidence for the H-atom elimination reaction in our experiment. Nevertheless, our observation of OCH_3 suggests that a C−C bond-breaking reaction must be a contributing step in the removal of carbon from a hydrocarbon surface under bombardment by hyperthermal atomic oxygen.

The dynamical behavior of the scattered OCH_3 reveals the qualitative nature of the C−C bond-breaking reaction. When the reactive scattering of OH and OCH_3 are compared (refer to ref 18 for OH), there are some common features. (1) The scattered products have mostly hyperthermal energies. (2) The translational energies of the hyperthermal products increase with increasing detection angles and with incident angle, for a given final angle. (3) The scattered product flux is largely specular. However, there are also some dramatic differences. (A) The average translational energies of scattered OCH_3 are much lower than those for scattered OH. (B) The fraction of OCH_3 that emerges from the surface at thermal velocities is much higher than this fraction for scattered OH. (C) The angular distribution of scattered OCH_3 is much broader than that for scattered OH. OH is formed through an H-atom abstraction reaction with a broad range of impact parameters. At collision energies similar to that used in the experiment described here, a spectator/stripping mechanism, with near perpendicular O−H−C configuration (large impact parameter), is the dominant mechanism for OH formation. However, OCH_3 is formed through C−C bond breakage. The results from theoretical studies of hyperthermal $O(^3P)$ with ethane, propane, and a hydrocarbon SAM surface[13−17] suggested two saddle points for C−C bond breakage, one with a collinear O−C−C geometry and one with a roughly perpendicular geometry. The barrier height for the collinear saddle point is about 193 kJ mol^{-1}, while an additional ∼50 kJ mol^{-1} is needed to surmount the perpendicular barrier. If C−C bond breakage were to proceed through a collinear reaction, then the OCH_3 would be expected to scatter backward in the CM frame. However, if C−C bond breakage occurred through the perpendicular transition state, then OCH_3 would be expected to scatter sideways in the CM frame. As the collision energy increases, theory suggests that C−C bond breakage favors the perpendicular geometry. Thus, at high

TABLE 2: Center-of-Mass Quantities Derived from a Kinematic Analysis of Inelastic Scattering of O_2 and Reactive Scattering of HO_2 (Hyperthermal Components) Following Impact of O_2 with $\theta_i = 60°$ and 30° on a Squalane Surface

incident angle		effective surface mass	collision energy	total final translational energy	total final internal energy
θ_i	scattered products	m_s (amu)	$\langle E_{coll} \rangle$ (kJ mol^{-1})	$\langle E_T \rangle$ (kJ mol^{-1})	$\langle E_{int} \rangle$ (kJ mol^{-1})
60°	O_2	60	662	393	269
	HO_2	80	725	268	457
30°	O_2	121	807	129	678
	HO_2	178	865	88	777

collision energies (e.g., this study), C−C bond breakage should be similar to a pure atom abstraction: An oxygen atom strips off a whole methyl group, with very little change in its initial momentum. The similarities between OCH_3 and OH scattering dynamics support this supposition.

To break a C−C bond, an incident O atom must interact strongly (a "hard hit") with a carbon atom. Therefore, the interaction time between the incoming O atom and the surface to form OCH_3 may be longer than the time to abstract an H atom during a grazing collision with the surface and form OH. Indeed, the effective surface masses for producing OCH_3 are much larger than those for producing OH (e.g., 124 amu vs 40 amu at $\theta_i = 60°$). As a consequence, the CM collision energies for the OCH_3 reaction mechanism are also much larger than those for OH, even though the incident O atoms have the same average translational energy. The energy partitioning is also dramatically different. For OH, most of the collision energy goes into translation, including the translational energy of OH and the recoiling surface fragment. For OCH_3, most of the collision energy goes into internal excitation of OCH_3 and the recoiling surface fragment. The partitioning of internal energy is not probed in our experiment. However, theoretical studies for gas-phase reactions of hyperthermal O(^{3}P) with small alkane molecules show that most of the internal energy goes into the hydrocarbon fragment that contains the incoming O atom.[13−15,19,20] It is thus possible that the initially formed OCH_3 is highly excited, especially given the large amount of energy that goes into internal excitation in the CM frame (374 kJ mol^{-1} for $\theta_i = 60°$).

As stated in section III.B, the direct reaction product, OCH_3, may dissociate to form H_2CO. The nascent OCH_3 or secondary H_2CO can be trapped on the surface, reach thermal equilibrium, and desorb with velocities characteristic of a Maxwell−Boltzmann distribution at the surface temperature. The thermal components of the TOF distributions for $m/z = 28$, 29, and 30 (flight time ~600 μs) may come from either trapped OCH_3 or H_2CO. If the nascent OCH_3 becomes trapped on the surface, the highly excited OCH_3 should be quenched rapidly on the surface and therefore would not dissociate into H_2CO. It might thus be expected that some OCH_3 products desorb thermally from the surface. The absence of thermal signals at $m/z = 15$ suggests that this process is not probable, although a small signal would have been indistinguishable from the noise. Ultimately, we cannot determine what fraction of products giving rise to the thermal components in the TOF distributions for $m/z = 28$, 29, and 30 comes from trapped OCH_3 and what fraction is from trapped H_2CO after rapid dissociation of OCH_3. Both products probably contribute. We assume that the H_2CO/OCH_3 ratio in the scattered products responsible for the hyperthermal signals is higher than the ratio for the thermal signals, because trapping at the surface provides a pathway for stabilization of internally excited OCH_3.

Products of C−C bond breakage other than OCH_3 were not identified in our experiments, either because they were not present or because they were produced at levels below our detection limits. The results from a theoretical calculation of hyperthermal O(^{3}P) reactions with a hydrocarbon SAM surface[15,17] suggest that the only other possible product from C−C bond breakage is ethoxy, but the reaction to produce ethoxy is highly improbable. On the SAM surface, the most accessible carbon atoms are those in the methyl group. The O atom has to have a hard hit on the carbon atom to break a C−C bond. Due to the steric effect, the probability of attacking the second or third carbon atom of the SAM chain and still having enough energy to overcome the reaction barrier is low. The probability of products from second or third C−C bond breakage scattering off the surface is even lower. Although squalane molecules were predicted in one study to orient such that their chain ends point up at the surface,[40] the squalane molecules in the liquid probably still have more mobility than the hydrocarbon chains on the SAM film. Therefore, incoming O atoms might strike a $-CH_2-$ group. However, if this reaction were to occur, the products would most likely be high-molecular-weight alkoxy and alkyl radicals that would remain in the liquid.[28] Even if these products did desorb, their velocities would be slow. We saw no slow signal at $m/z = 30$, and assuming reaction with a $-CH_2-$ group is not probable, these reaction products would be undetectable given the uncertainties in our experiment. We do not believe that high-molecular-weight alkoxy or alkyl reaction products are responsible for the slow signals that we attributed to collision-induced evaporation of squalane, because related experiments in which hyperthermal Ar atoms were directed at a liquid surface also showed substantial evidence for collision-induced evaporation.

A final point of discussion involves the possible role of intersystem crossing from O(^{3}P) to O(^{1}D) in the C−C bond-breaking channel. Triplet−singlet intersystem crossing has been reported in studies of O(^{3}P) reactions with CH_3I,[41] cyclohexane clusters,[42] organized organic thin films,[43] and liquid saturated hydrocarbons.[44] The importance of intersystem crossing varies with reactants and with collision energy, increasing with the longer residence times that reactants spend in the crossing region and decreasing with higher collision energies. At hyperthermal collision energies, triplet−singlet crossing plays negligible roles in the reactions of O(^{3}P) with H_2[33] and CH_4.[16] For reactions of O(^{3}P) with hydrocarbons, CH_2OH would be an expected product if intersystem crossing occurred and the reaction took place by an insertion reaction through an alcohol intermediate. However, if intersystem crossing occurred on the liquid surface, then the intermediate complex might be stabilized on the surface and leave an alcohol product.[23] For the current study of hyperthermal O(^{3}P) with a squalane surface, the absence of signals from a volatile CH_2OH product indicates that either the intersystem crossing is negligible or the alcohol products are stabilized on the surface. In any case, intersystem crossing does not affect the dynamical behavior of the scattered methoxy radical.

B. O_2 Reaction with Squalane To Produce HO_2. The dynamical behavior of reactively scattered HO_2 is similar to that of inelastically scattered O_2. Both scattered products have predominantly hyperthermal translational energies, and the translational energies of both scattered products increase with increasing final angle and with incident angle (for a given final angle). In addition, the products are scattered forward, nominally in the specular direction. The observed scattering behavior of

O_2 and HO_2 is qualitatively similar to the scattering behavior of O and OH, reported in ref 18, which led to the conclusion that the OH radical is formed by a direct abstraction mechanism. Likewise, we conclude that the scattering dynamics of HO_2 indicate a direct abstraction mechanism, where an incident O_2 molecule abstracts a hydrogen atom in a gas-phase-like collision with a local region of the surface.

We observed earlier that inelastic scattering of O and reactive scattering of OH showed almost identical dynamics. Such similar dynamics were not surprising in this case where a relatively heavy O atom abstracts a light hydrogen atom and the reaction barrier and exoergicity are low, approximately 28.9 and -9.6 kJ mol^{-1}, respectively, for abstraction of primary H atoms.[21] However, there are some significant quantitative differences in the inelastic scattering of O_2 and reactive scattering of HO_2. In the laboratory frame, the average translational energies of scattered HO_2 are only about 75% of those for O_2. The ratio of thermal to hyperthermal scattering for HO_2 is greater than that for O_2, and the flux angular distribution for hyperthermal HO_2 is broader than that for O_2. When viewed in the CM reference frame, the effective surface mass for reactive scattering to produce HO_2 is significantly higher than that for inelastic scattering of O_2, and the fraction of the CM collision energy that goes into translation is also much smaller for the HO_2 channel than for O_2 scattering. These dynamical differences can be explained by the high reaction barrier. For H-atom abstraction by O_2, the barrier is at least as high as the endoergicity, which is $\sim$206 kJ mol^{-1}. With a higher reaction barrier, the requirement for the collision geometry of a successful reaction is more stringent. Thus, O_2 collisions that produce HO_2 are expected to be more "head-on," with a large component of the collision energy directed along the line of centers between an O atom in the O_2 molecule and an H$-$C moiety on the surface. The preponderance of head-on collisions in the formation of HO_2 would be expected to lead to broader angular distributions for HO_2 than those exhibited by inelastically scattered O_2, because there are no restrictions on the collision geometry for inelastically scattered O_2. For inelastic scattering of O_2, large-impact-parameter collisions will dominate, so the O_2 should be scattered predominantly in the forward direction. Head-on collisions and a high endoergicity will also lead to final HO_2 translational energies that are smaller than those for inelastically scattered O_2. Furthermore, the unique features of the collisions that produce HO_2 should enhance its thermal equilibration with the surface over that of inelastically scattered O_2, which accounts for the higher thermal component in the HO_2 TOF distributions versus the O_2 TOF distributions.

Another difference between H-atom abstraction by O and O_2 is the second H-atom abstraction to form H_2O or H_2O_2. H_2O is an important reaction product when squalane is bombarded with O(^{3}P) atoms.[18,28] The formation of H_2O is explained by a secondary reaction in which the nascent OH radical abstracts a hydrogen atom from another portion of the surface. This reaction has a low barrier of less than 5 kJ mol^{-1}.[45,46] The scattered H_2O molecules may possess translational energies that are hyperthermal or thermal (given by the surface temperature). Signals indicative of an analogous process where HO_2 abstracts an H atom to form H_2O_2 were not observed in our experiments. This secondary reaction may be improbable, as the endoergicity of H-atom abstraction by HO_2 to form H_2O_2 is $\sim$66 kJ mol^{-1}.

V. Conclusion

We have identified a direct C$-$C bond-breaking reaction resulting from the interaction of hyperthermal O(^{3}P) atoms with a saturated hydrocarbon (squalane) surface. This reaction leads to the formation of methoxy, OCH_3, which may be ejected from the surface. The initially formed OCH_3 is probably highly internally excited and may undergo secondary dissociation to form H_2CO. The dynamics of the C$-$C bond-breaking product were studied by measuring translational energy and angular distributions of the product detected at $m/z = 30$. Whether OCH_3 survived to the detector or dissociated to H_2CO, the observed dynamics reflect the nascent OCH_3, as the H_2CO will hardly deviate from the velocity and direction of the parent OCH_3 when a light hydrogen atom recoils. We observed no evidence for the hydroxymethyl radical, CH_2OH, which could have been formed either directly or through isomerization of OCH_3. OCH_3 (or its daughter, H_2CO) may scatter directly from the surface with hyperthermal energy, or it may be trapped on the surface and desorb thermally with velocities characteristic of the surface temperature. The dynamical behavior of direct C$-$C bond breakage has been described in the CM reference frame with the use of a kinematic picture (Newton diagram) that allows the determination of the effective surface mass encountered by the incident O atom, the CM collision energy, and the fraction of the CM collision energy that is converted to internal energy in the surface and in the recoiling gaseous species.

In addition to characterizing the dynamics of the O(^{3}P) reaction to produce OCH_3, we have also identified and characterized the dynamics of the reaction of O_2 (the minor component of our hyperthermal oxygen beam) with squalane to produce HO_2. This reaction exhibits dynamics that are substantially different from H-atom abstraction at a squalane surface by O atoms and are also different from O_2 inelastic scattering on a squalane surface.

Acknowledgment. This work was supported primarily by a grant from the Department of Defense Experimental Program for the Stimulation of Competitive Research, administered by the Air Force Office of Scientific Research (Grant No. FA9550-04-1-0428). Additional support came from an Air Force Office of Scientific Research Multidisciplinary University Research Initiative (Grant No. F49620-01-1-0335).

References and Notes

(1) Minton, T. K.; Garton, D. J. Dynamics of Atomic-Oxygen-Induced Polymer Degradation in Low Earth Orbit. In *Chemical Dynamics in Extreme Environments*; Dressler, R., Ed.; Advanced Series in Physical Chemistry 11; World Scientific: Singapore, 2000, pp 420$-$489.

(2) English, L. K. *Mater. Eng.* **1987**, (Aug), 39.

(3) Hunton, D. E. *Sci. Am.* **1989**, *261*, 92.

(4) Murad, E. *J. Spacecr. Rockets* **1996**, *33*, 131.

(5) Kenneth, T. N.; Minton, T. K.; Sibener, S. J. *J. Phys. Chem. B* **2005**, *109*, 8476.

(6) Kenneth, T. N.; Sibener, S. J.; Minton, T. K. *High Perform. Polym.* **2004**, *16*, 197.

(7) Kenneth, T. N.; Minton, T. K.; Sibener, S. J. *Prog. Org. Coat.* **2003**, *47*, 443.

(8) Zhang, J.; Minton, T. K. *High Perform. Polym.* **2001**, *13*, S467.

(9) Kinoshita, H.; Umeno, M.; Tagawa, M. *Surf. Sci.* **1999**, *440*, 49.

(10) Ngo, T.; Snyder, E. J.; Tong, W. M.; Williams, R. S.; Anderson, M. S. *Surf. Sci.* **1994**, *314*, L817.

(11) Gindulyte, A.; Massa, L.; Banks, B. A.; Rutledge, S. K. *J. Phys. Chem. A* **2000**, *104*, 9976.

(12) Garton, D. J.; Minton, T. K.; Troya, D.; Pascual, R. Z.; Schatz, G. C. *J. Phys. Chem. A* **2003**, *107*, 4583.

(13) Troya, D.; Pascual, R. Z.; Schatz, G. C. *J. Phys. Chem. A* **2003**, *107*, 10497.

(14) Troya, D.; Pascual, R. Z.; Garton, D. J.; Minton, T. K.; Schatz, G. C. *J. Phys. Chem. A* **2003**, *107*, 7161.

(15) Troya, D.; Schatz, G. C. *Int. Rev. Phys. Chem.* **2004**, *23*, 341.

(16) Troya, D.; Schatz, G. C.; Garton, D. J.; Brunsvold, A. L.; Minton, T. K. *J. Chem. Phys.* **2004**, *120*, 731.

(17) Troya, D.; Schatz, G. C. *J. Chem. Phys.* **2004**, *120*, 7696.

(18) Zhang, J.; Garton, D. J.; Minton, T. K. *J. Chem. Phys.* **2002**, *117*, 6239.
(19) Yan, T.; Doubleday: C.; Hase, W. L. *J. Phys. Chem. A* **2004**, *108*, 9863.
(20) Yan, T.; Hase, W. L.; Doubleday: C. *J. Chem. Phys.* **2004**, *120*, 9253.
(21) Andresen, P.; Luntz, A. C. *J. Chem. Phys.* **1980**, *72*, 5842.
(22) Garton, D. J.; Minton, T. K.; Alagia, M.; Balucani, N.; Casavecchia, P.; Volpi, G. G. *J. Chem. Phys.* **2000**, *112*, 5975.
(23) Garton, D. J.; Minton, T. K.; Alagia, M.; Balucani, N.; Casavecchia, P.; Volpi, G. G. *Faraday Discuss.* **1997**, *108*, 387.
(24) Kelso, H.; Kohler, S. P. K.; Henderson, D. A.; McKendrick, K. G. *J. Chem. Phys.* **2003**, *119*, 9985.
(25) Kohler, S. P. K.; Allan, M.; Kelso, H.; Henderson, D. A.; McKendrick, K. G. *J. Chem. Phys.* **2005**, *122*, 024712.
(26) Kohler, S. P. K.; Allan, M.; Costen, M. L.; McKendrick, K. G. *J. Phys. Chem. B* **2006**, *110*, 2771.
(27) Li, G.; Bosio, S. B. M.; Hase, W. L. *J. Mol. Struct.* **2000**, *556*, 43.
(28) Schatz, G. C. Northwestern University, Evanston, IL. Personal communication, 2006.
(29) Lee, Y. T.; McDonald, J. D.; LeBreton, P. R.; Herschbach, D. R. *Rev. Sci. Instrum.* **1969**, *40*, 1402.
(30) O'Laughlin, M. J.; Reid, B. P.; Sparks, R. K. *J. Chem. Phys.* **1985**, *83*, 5647.
(31) Garton, D. J.; Brunsvold, A. L.; Minton, T. K.; Troya, D.; Maiti, B.; Schatz, G. C. *J. Phys. Chem. A* **2006**, *110*, 1327.
(32) Caledonia, G. E.; Krech, R. H.; Green, D. B. *AIAA J.* **1987**, *25*, 59.
(33) Garton, D. J.; Minton, T. K.; Maiti, B.; Troya, D.; Schatz, G. C. *J. Chem. Phys.* **2003**, *118*, 1585.
(34) *NIST Chemistry WebBook*; National Institute of Standards and Technology: Gaithersburg, MD. http://webbook.nist.gov/chemistry.
(35) Brunsvold, A. L.; Upadhyaya, H. P.; Zhang, J.; Minton, T. K. Manuscript in preparation.
(36) Wodtke, A. M. Ph.D. Thesis, University of California, 1986.
(37) Lin, J. J.; Lee, Y. T.; Yang, X. *J. Chem. Phys.* **1998**, *109*, 2975.
(38) Garton, D. J. Ph.D. Thesis, Montana State University, 2004.
(39) Minton, T. K.; Giapis, K. P.; Moore, T. *J. Phys. Chem. A* **1997**, *101*, 6549.
(40) Harris, J. G. *J. Phys. Chem.* **1992**, *96*, 5077.
(41) Alagia, M.; Balucani, N.; Cartechini, L.; Casavecchia, P.; van Beek, M.; Volpi, G. G.; Bonnet, L.; Rayez, J. C. *Faraday Discuss.* **1999**, *113*, 133.
(42) Rudich, Y.; Hurwitz, Y.; Lifson, S.; Naaman, R. *J. Chem. Phys.* **1993**, *98*, 2936.
(43) Paz, Y.; Trakhtenberg, S.; Naaman, R. *J. Am. Chem. Soc.* **1994**, *116*, 10344.
(44) Patino, P.; Hernandez, F. E.; Rondon, S. *Plasma Chem. Plasma Process.* **1995**, *15*, 159.
(45) Huynh, L. K.; Ratkiewicz, A.; Truong, T. N. *J. Phys. Chem. A* **2006**, *110*, 473.
(46) Donahue, N. M.; Anderson, J. G.; Demerjian, K. L. *J. Phys. Chem. A* **1998**, *102*, 3121.